Quantum magnetotransport in a mesoscopic antidot lattice

I. V. Zozulenko, Frank A. Maaø, and E. H. Hauge
Institutt for Fysikk, Norges Tekniske Høgskole, N-7034, Trondheim, Norway
(Received 19 September 1994)

The effect of a perpendicular magnetic field on quantum electron transport in a periodic array of antidots is studied. On the basis of a recursive Green-function technique the conductance of the finite antidot lattice is calculated in the framework of the Landauer-Büttiker formalism. The dependence of the conductance of the finite array on the Fermi energy and the magnetic field can be understood from an analysis of the band structure of the corresponding infinite strip superlattice. The latter is shown to consist of quasiparabolic Bloch states and almost dispersionless bands representing the bulk Landau states and quasibound states around antidots. The particle current density associated with these bands is calculated. The quasiparabolic band corresponds to propagation in magnetic edge states, whereas antidot bands correspond to counterclockwise rotation *around single antidots*. Landau bands, on the other hand, correspond to the counterclockwise rotation in the space *between antidots*. It is shown that the particle current flow in Landau and antidot states can have a maximum near the lower edge of the strip, i.e., opposite to that which is normally expected. The physical reason for this is given. The magnetoconductance through the finite array of antidots is shown to exhibit plateaulike behavior when electrons propagate in the magnetic edge state, and irregular oscillating behavior corresponding to propagation in Landau or antidot bands. The latter is due to strong mode mixing at the boundary of the array.

During the past few years, magnetotransport in a two-dimensional electron gas (2DEG) with a carefully engineered periodic potential has been the topic of extensive studies, both experimental[1–16] and theoretical.[5,8,17–27] In particular, a number of experiments have been reported where a controllable 2D potential with a grating constant of the order of 200 nm – 1 μm is applied to a high-mobility 2DEG defined on a GaAs-$Al_xGa_{1-x}As$ interface. By changing the strength of the modulation potential, one can achieve a transition from weak density variations of the 2DEG to the formation of completely depleted regions, i.e., arrays of quantum antidots. In relatively high magnetic fields, $B \gtrsim 1$ T, the longitudinal magnetoresistance of the lateral superlattices, like that of unmodulated 2DEG, exhibits the usual Shubnikov–de Haas oscillation with a period proportional to $1/B$, reflecting the Landau energy spectrum. In lower magnetic field, when the classical cyclotron radius $r_c = \hbar k_F/eB$ at the Fermi momentum $\hbar k_F$ is commensurate with a superlattice period, a rich variety of effects has been detected. In the case of a weak modulation potential a new type of magnetoresistivity oscillations, also periodic in $1/B$, was found.[1,4–6,10] These oscillations have been attributed to the formation of a Hofstadter-type energy spectrum[28] due to the presence of a superlattice potential.[5,18,24,26] The 2DEG subjected to the strong modulation potential exhibits an entirely different behavior. The resonances in longitudinal magnetoresistance found in Refs. 2, 3, 6–10, and 12–16 have been interpreted in the framework of classical chaotic electron orbits trapped around or in between groups of antidots[19,20,25] and in terms of band conductivity.[27]

So far, most of the experimental and theoretical studies of magnetotransport in a two-dimensional periodic potential have been concentrated on essentially *macroscopic* structures. In such systems the phase coherence length λ_ϕ, as well the elastic mean free path λ_l, are much smaller than the size of the sample. In this case phase-breaking events destroy coherence, and magnetotransport through the device can be described in the framework of the Drude model.[29] Recently, however, Schuster *et al.*[15] studied the magnetotransport in a *mesoscopic* antidot array in the confined geometry with characteristic dimension smaller than both λ_ϕ and λ_l. As phase coherence in mesoscopic structures is preserved over the entire device, their transport properties are clearly distinct from those of macroscopic ones, and have to be analyzed on the basis of the Landauer-Büttiker formalism.[30,31] In this case transport in the leads is dominated by magnetic edge states, and the linear longitudinal two-terminal conductance is given as $G = 2(e^2/h)\sum_{\alpha,\beta}|t_{\alpha,\beta}|^2$, where $t_{\alpha,\beta}$ is the scattering matrix at the Fermi energy E_F from incoming state α to transmitted state β. In the absence of the antidot array, the conductance of the homogeneous quantum wire is simply proportional to the number of propagating states.

Until now, the theory of magnetotransport in 2D periodic mesoscopic structures of confined geometries has been developed for the case of a weak modulation potential[17,23] and for coupled quantum dot arrays,[22] the structure of which is complementary to that of antidots. A theoretical description of magnetotransport in a strip geometry of finite width, with a strong modulation potential (antidot arrays) is still missing, and the present paper represents a step in this direction. Our calculation are, so far, limited to the extreme quantum regime with a few Landau levels in the leads. In contrast, in antidot arrays studied by Schuster *et al.*,[15] the period of the superlattice

was much bigger than the Fermi wavelength λ_F (corresponding to roughly 10 Landau levels in the leads at $B \sim 1$ T). In this case the classical picture of commensurable orbits and chaotic trajectories[19,20] appeared to be valid, even for mesoscopic arrays of quantum antidots. However, phase coherence effects manifest themselves in the reproducible quantum fluctuations (believed to be caused by the Aharonov-Bohm effect) superimposed onto classical resonances. One can expect that further advances in nanofabrication technology will soon make it possible to approach the true quantum limit, when λ_F is comparable or even greater than the period of the superlattice.

We calculate the longitudinal conductance in the simplest possible two-terminal geometry and show that the transmission characteristics of the *finite* structure can be explained from the viewpoint of electron propagation in the *infinite* arrays. This is the essence of our approach. We calculate the band structure of the antidot lattice and study the current density associated with different states. We show that three types of states are possible in the antidot lattice: magnetic edge states located at the boundaries, and two types of bulk states, antidot and Landau states. In these bulk states electrons perform counterclockwise motion, around single antidots and in the space between antidots, respectively. The magnetoconductance of the finite antidot lattice is then analyzed on the basis of the band structure of the corresponding infinite structure.

The geometry of our device is shown in Fig. 1. We consider an infinite strip of width Na (with a being the lattice constant of the underlying tight-binding lattice), confined by hard walls in the transverse direction and placed in the perpendicular magnetic field B. Choosing the Landau gauge $\mathbf{A}=(-Ban,0,0)$ and following Peierls in incorporating the magnetic field by a phase factor on the hopping amplitudes, we arrive at the tight-binding Hamiltonian[32]

$$H=\sum_{m,n}\Big(|m,n\rangle(\epsilon_0+V_{m,n})\langle m,n| - t\{|m,n\rangle\langle m,n+1| + |m,n\rangle e^{2\pi i f n}\langle m+1,n| + \text{H.c.}\}\Big) \qquad -\infty<m<\infty,\ 1\le n\le N. \quad (1)$$

Here $V_{m,n}$ is the periodic potential (to be specified below) with the period La defined in the finite region of the infinite strip, t is the nearest-neighbor hopping amplitude at zero magnetic field, ϵ_0 is the lattice site electron energy, and $f \equiv eBa^2/h$ is the dimensionless magnetic field. In the presentation of our results, instead of f, we use $\Phi/\Phi_0 \equiv L^2 f$, which is the magnetic flux per superlattice unit cell, $\Phi = (La)^2 B$, divided by the flux quantum, $\Phi_0 = h/e$. In our calculations, for convenience, we set $\epsilon_0 = 0$, and give the energy in units of t. We could equally well have set $\epsilon_0 = 4t$ with $t = \hbar^2/2m^*a^2$, m^* being the effective mass. From this choice it is evident that, in the continuum limit, it is equivalent to the effective mass approximation.

In order to calculate the scattering matrix $t_{\alpha,\beta}$ and, thereby, the Landauer-Büttiker conductance G, we use standard recursive Green-function techniques,[31,33,34] starting from the surface Green function in a magnetic field. We consider an antidot superlattice defined in a finite region of the strip of width $N = 47$ and containing six 2×2 antidots in the one-dimensional (1D) elementary unit cell (see Fig. 1). Each antidot is modeled by a hard-wall potential. The conductance G of a short array with $\mathcal{M} = 8$ 1D unit cells as a function of E_F is given for two different values of the relative flux, Φ/Φ_0, in Figs. 2(b)

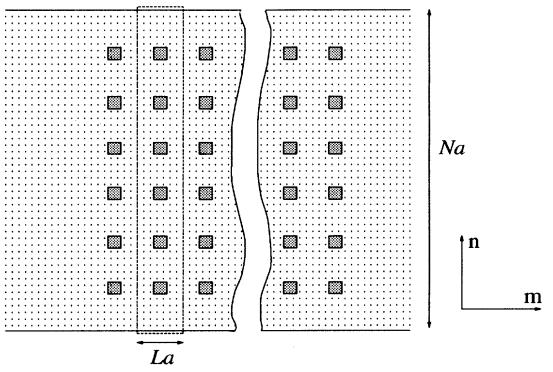

FIG. 1. Schematic geometry of the device. Lattice sites of an infinite strip of width Na are denoted by points. Shaded squares correspond to the periodic antidot potential with the period La defined in a finite region of the strip. The dashed-line rectangle indicates the one-dimensional elementary unit cell of the antidot lattice.

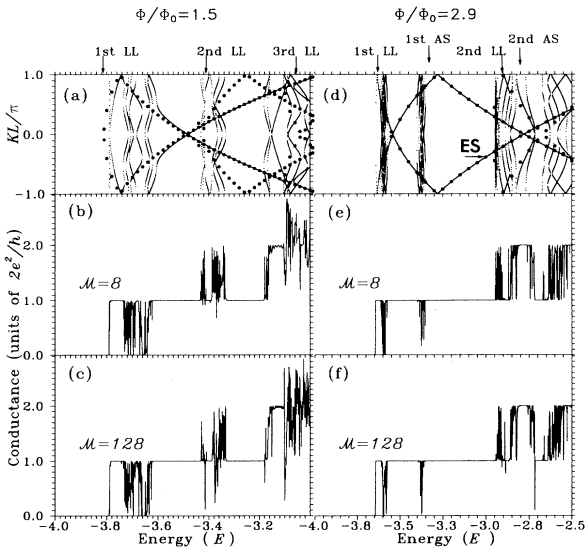

FIG. 2. Band structure of the infinite antidot superlattice in reduced zone representation [(a), (d)]; the large points correspond to the dispersion relations for the *homogeneous* wire (without an antidot potential). Conductance of a finite antidot structure with $\mathcal{M} = 8$ one-dimensional unit cells [(b), (e)], and a quasi-infinite one with $\mathcal{M} = 128$ unit cells [(c), (f)]. The relative flux is $\Phi/\Phi_0 = 1.5$ and 2.9 for the left and right panels, correspondingly.

and 2(e). Corresponding results for the quasi-infinite array with $\mathcal{M} = 128$, are shown in Figs. 2(c) and 2(f). The qualitative features are similar, and this motivates a study of the magnetic Bloch states in an *infinite* array. Under the gauge chosen, the magnetic unit cell (in the m direction) coincides with the superlattice period La and we appeal to Bloch's theorem looking for solutions to the Schrödinger equation which have the form of a plane wave times a function with the periodicity of the antidot lattice L,[35]

$$\psi(m,n) = e^{iKm}\, u(m,n); \quad u(m+L,n) = u(m,n). \qquad (2)$$

Using the transfer matrix technique we calculate the band structure $E = E(K)$. The results are shown in Figs. 2(a,d). Two types of bands are clearly distinguishable: quasiparabolic Bloch states and almost dispersionless minibands.

We first discuss the quasiparabolic Bloch states. Fat points in Figs. 2(a,d) indicate the dispersion relations for the corresponding *homogeneous* strip (without the antidot potential). In the homogeneous strip the propagating states (except in Landau bands) are the edge states located in the vicinity of the upper boundary (right moving state) or the lower boundary (left moving state). For an illustration, see Ref. 32. If the magnetic field is strong enough, the transverse extent [which is of the order of the magnetic length, $l_B = (\hbar/eB)^{1/2}$] of the edge state can be smaller than the distance between the boundary and the nearest antidot row. In this case the edge state does not feel the presence of the antidots at all and, consequently, its dispersion is the same with and without antidots. Conversely, with larger l_B or with several edge states increasingly removed from the boundary, one or more edge states of the homogeneous strip may be blocked by the presence of the antidots. This is illustrated in the energy region $-3.5 \lesssim E \lesssim -3.1$ in Fig. 2(a), when two propagating states exist in the homogeneous strip, but only one of them can propagate in the strip with antidots. Thus the number of propagating quasiparabolic edge states in the antidot structure equals the number of edge states (in the corresponding homogeneous strip) with transverse localization length less than the distance between the antidots and the boundary.

Next, we discuss the origin of essentially dispersionless states. In Fig. 2 the arrows labeled LL indicate the position of the conventional bulk Landau levels, $E_{\rm LL} = \hbar\omega_c(n+\frac{1}{2})$, with $\omega_c = eB/m^*$ the cyclotron frequency. The transformation of the Landau levels into Landau bands due to the presence of the periodic potential is clearly evident. At high magnetic fields another type of miniband appears, Fig. 2(d). We attribute these minibands to quasibound states around a single antidot. To support this interpretation we have solved the eigenvalue problem of the continuous Schrödinger equation with a single antidot modeled by a hard-wall circular potential. The two lowest bound states are indicated in Fig. 2(d) by arrows marked AS. The lower the magnitude of the magnetic field, the greater the spatial extent of the antidot quasibound state. If the distance between neighboring antidots is smaller than the radius of the quasibound state, the latter cannot exist in an antidot superlattice. This is the case for the low-field results displayed in Figs. 2(a)–2(c).

Each antidot miniband consists of six states, which equals the number of antidots in the 1D unit cell of the superlattice, whereas each Landau miniband consists of seven states, which equals the number of the open spaces between antidots; see Figs. 3(a,b). We found a remarkable similarity between the miniband fine structure and dispersion relations of the *homogeneous* strip with the corresponding number of unit cells.[32] The correspondence between the antidot miniband in Fig. 3(a) and the corresponding band in a homogeneous tight-binding strip of width $N = 6$ in Fig. 3(c) is almost perfect, except for the fact that dispersion curves in Fig. 3(a) show anticrossing with the edge-state dispersion curve. This similarity is not accidental. Indeed, each antidot can be considered as an elementary cell in an effective tight-binding strip where the lattice constant is equal to the distance between antidots, lattice site electron energies correspond to the energy of the quasibound state around a single antidot, and the magnitude of the hopping amplitude, $|t'|$, is determined by the overlap between the neighboring quasibound states. This interpretation is supported by the fact that also the miniband of Fig. 2(b), corresponding to the seven states *between* the dots, is very similar to that of Fig. 2(c), once the appropriate shift of KL by π, due to the different position of the states in the unit cell, has been made. In the tight-binding approximation the width of minibands is proportional to $|t'|$ (and, in zero magnetic field is equal to $8|t'|$). With increasing field or lowered energy, the quasibound states becomes more localized. This reduces the overlap, and, consequently, the width of miniband. This effect of narrowing minibands is seen in Figs. 2(a,d).

The states in the effective tight-binding model are all states rotating in a counterclockwise direction. Therefore, hopping between two such neighboring states, the electron acquires a phase shift of π. This implies that the corresponding hopping amplitudes has the opposite sign from that in the usual tight-binding model. In the homogeneous tight-binding strip of width N at high mag-

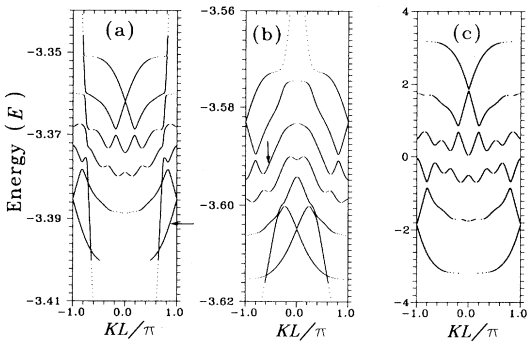

FIG. 3. Closeup of the band structure of the antidot lattice representing (a) the lowest circular state around an antidot and (b) the lowest Landau level [both are the same as in Fig. 2(d) but in enlarged scale]. (c) The dispersion relation for the *homogeneous* tight-binding strip of width $N = 6$.

netic field there exist N edge states moving in the same direction. The lowest-energy right-moving state is located near the upper edge, and the center of the mass of each subsequent state is shifted down toward the lower edge. Due to the opposite sign of the hopping amplitude (which corresponds to the opposite sign of the effective mass of the quasiparticle), the situation is reversed in our effective tight-binding model. The lowest energy state is located in the vicinity of the *lower* edge and the location of each subsequent state is shifted upward to the upper edge of the strip.

To confirm the above picture of the origin of the minibands in the antidot structure, we calculated the spatial distribution of the particle current associated with the different types of Bloch states. Fundamentally, the current in our model is associated with hopping along *bonds*.[32] Nevertheless, for visualization purposes it is more convenient to view the local current density $\boldsymbol{j}(m,n)$ as a vector associated with *sites*. The corresponding expression is derived in standard fashion from a combination of the time-dependent Schrödinger and the continuity equation. It reads

$$\begin{aligned}\boldsymbol{j}_{K,\alpha}(m,n) = \frac{it}{2a\hbar}\{&\hat{\mathbf{m}}\,\psi^*_{K,\alpha}(m,n)[e^{2\pi i f n}\psi_{K,\alpha}(m+1,n)\\ &-e^{-2\pi i f n}\psi_{K,\alpha}(m-1,n)]\\ &+\hat{\mathbf{n}}\,\psi^*_{K,\alpha}(m,n)[\psi_{K,\alpha}(m,n+1)\\ &-\psi_{K,\alpha}(m,n-1)] - \text{c.c.}\},\end{aligned} \tag{3}$$

where $\psi_{K,\alpha}$ is the wave function associated with the state α and $\hat{\mathbf{m}}$,$\hat{\mathbf{n}}$ are the unit vectors in the longitudinal and transverse directions. In the continuum limit Eq. (3) reduces to the standard definition of the current density in a magnetic field.[36]

In Fig. 4 the particle current density pattern in the infinite antidot lattice is shown for three different types of states. Figure 4(a) represents a right-moving edge state corresponding to the quasiparabolic band. In this case the magnetic field pushes electrons to the upper boundary of the strip, separating them from the area containing the antidot potential. In the case of flat bands the current density pattern corresponds, as expected, to the counterclockwise electron rotation around an antidot (for the antidot miniband) or in the space between antidots (for the Landau miniband); see Figs. 4(b,c). Here we show the particle density flow only for one selected state in the antidot and Landau minibands. For the other states in these bands the current density pattern has the same character (i.e., corresponds to electrons rotating counterclockwise around or between antidots) but different states have different transverse localizations. If an electron belongs to the state at the top of the miniband, the particle flow has, as expected, its maximum at the upper row of antidots and is negligible small in other parts of the superlattice. Going down through the miniband states, the maximum of the current density is shifted downwards by one row of antidots at a time and, eventually, electrons belonging to the lowest energy state move close to the lower boundary of the strip. Note that similar propagating states located at the unusual position in the strip have been discovered in arrays of coupled quantum dots[22] and in a quantum wire containing a periodic weak modulation potential.[23] In these structures such states are shown to be responsible for predicted exotic behavior of the Hall conductance which can be fractional or negative even in a one-electron picture. Thus similar effects can be expected in the quantum antidot arrays in a Hall bar geometry. We defer this issue to future publications.

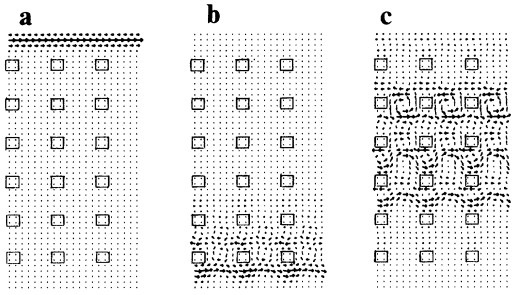

FIG. 4. Particle current density in an infinite antidot lattice associated with (a) the right-moving edge state [horizontal arrow marked by ES in Fig. 2(d)]; (b) the antidot state [marked by an arrow in Fig. 3(a)]; and (c) the Landau state [marked by an arrow in Fig. 3(b)].

Having calculated the band structure of the infinite antidot lattice, we can interpret the dependence of the conductance of the finite antidot structure [Figs. 2(b,e)] as follows. When the Fermi energy of incoming electrons lies in the range corresponding to edge-state propagation, the transmission exhibits a plateaulike dependence on energy. The plateau index is quantized and equal to the number of edge states with positive velocity in the corresponding infinite antidot lattice. In this case the transport through a finite antidot lattice is completely adiabatic because the edge state in the potential-free region and the edge state in the region with antidot potential are characterized by the same dispersion relation.

When the Fermi energy hits the regions where the current is carried by flat bands, the conductance is no longer quantized. In this case incoming edge states in the potential-free region, when entering the region with antidot potential, have to be redistributed between the bulk antidot (or Landau, depending on the energy) states. This leads to strong mode mixing, which causes the irregular behavior of the conductance. The maximum value of the conductance oscillations is given by the number of propagating states impinging on the superlattice, whereas the minimum value of these oscillations can drop to zero. The width of the oscillation peaks and dips becomes narrower with increasing number of antidot cells. For the case of a semi-infinite antidot lattice [$\mathcal{M} = 128$; Figs. 2 (c,f)], some of them are even unresolved on the scale of the figure. Note that the Landauer formula, strictly speaking, is valid when the voltage difference between right and left reservoirs is small in comparison with the energy difference that cause characteristic changes in the transmission coefficient.[37] In practice, with a finite voltage, the sharp peaks and dips in the regions with irregular oscillating behavior will be averaged out, with

a resultant drop in the magnetoconductance (increase of the magnetoresistance), in comparison with regions where the current is carried by the edge states.

In most experiments one varies the magnetic field rather than the Fermi energy of the electrons. The above analysis of the dependence of conductance on the Fermi energy can be directly applied to the interpretation in Fig. 5, which shows the conductance of a finite lattice with $\mathcal{M} = 8$ as a function of the relative flux Φ/Φ_0, at the given energy $E = -3.6$. Again, the dependence of the conductance on the magnetic field shows plateau regions with integer index and regions of fluctuating irregular behavior. The latter corresponds to electron propagation in the bulk (antidot or Landau, depending on the energy) bands, whereas plateau regions are attributed to edge-state propagation. We would like to stress that the regions of irregular conducting oscillations correspond to the circular motion around *single* antidots (or in the quantum dot defined by the space *between four antidots*). Different regions should be associated with the different quantum numbers of a quasibound state around *single* antidots (or *between four antidots*). It is not clear how to reconcile the classical interpretations of detected magnetoresistance maxima in antidot structures in terms of pinned electron orbits around groups of four and more antidots[7,8,12,15,16] with the Bloch theorem, which reflects the translational symmetry of a single period of antidot superlattice.

In our calculation we modeled antidots by an idealized hard-wall potential. In real quantum structures the precise form of the potential landscape is unknown. Theoretical calculations based on self-consistent solutions of the Poisson equation indicate that actual potentials can be approximated by parabolic or saddle-shaped confinement.[38] We performed calculations of the magnetoconductance of an antidot lattice with a soft cosine-type potential and found qualitative agreement with the case of the hard-wall potential. Our model is also idealized in the sense that identical antidots form a perfect superlattice. Irregularities of the lattice as well as of individual antidots can reduce perfect backscattering or suppress resonance transmission in the region of bulk state propagation. This issue will be addressed elsewhere.

Finally, a word of caution: our results cannot yet be compared directly to existing experiments, since our parameter values and those of the experiments are still significantly different. As a numerical example, choose $\lambda_F = 150$ nm (which corresponds to the sheet electron density $N_s = 3 \times 10^{14}$ m^{-2}). For $E = -3.6$ (as in Fig. 5), this corresponds to the antidot diameter $d \approx 22$ nm, a superlattice period $La \approx 105$ nm, and a region of magnetic field variation $0 < B < 0.6$ T. Such a set of parameters of the antidot lattice has not yet been achieved technologically. Therefore further miniaturization of actual devices as well as a reduction of the sheet electron density is needed to approach the true quantum limit, when λ_F is comparable to the period of superlattice. Conversely, a calculation which could reliably incorporate ~ 10 Landau levels with a realistic array geometry would, with the present technique, be forbiddingly large. However, we are confident that theory and experiment will move considerably closer to one another in the near future.

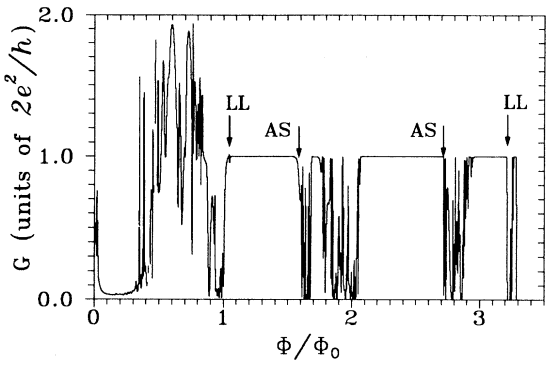

FIG. 5. Conductance of the finite antidot structure with $\mathcal{M} = 8$ one-dimensional unit cells as a function of the relative flux Φ/Φ_0. Arrows indicate the positions of the lowest bulk Landau levels (LL) and the bound states around a single antidot (AS); $E = -3.6$.

In conclusion, we have presented a study of the magnetoconductance of an antidot superlattice structure. The conductance of the finite lattice is interpreted on the basis of the band structure of the corresponding infinite strip of antidot lattice. Three types of bands are found: quasiparabolic ones corresponding to edge-state propagation, and flat bands corresponding to bulk antidot and Landau states. It is shown that the particle current flow in Landau and antidots states can have a maximum near the lower boundary of the strip, i.e., opposite to that which is normally expected. The physical reason for this is given. The magnetoconductance is shown to exhibit plateaulike behavior when electrons propagate in magnetic edge states, and complicated irregular oscillating behavior in the case of propagation in Landau or antidot bands.

Although our parameter values are still somewhat different from those of existing experiments, this gap will probably be closed before long. In any case, we believe that we have presented a conceptual framework which will prove fruitful in the discussion of coherent magnetotransport through periodic arrays of antidots in the quantum regime.

A fruitful discussion with Professor J. P. Kotthaus is gratefully acknowledged. One of the authors (I.V.Z.) wishes to thank Norges Forskningsråd for financial support.

[1] E. S. Alves, P. H. Beton, M. Henini, L. Eaves, P. C. Main, O. H. Hughes, G. A. Toombs, S. P. Beaumont, and C. D. W. Wilkinson, J. Phys. Condens. Matter **1**, 8257 (1989).

[2] K. Ensslin and P. M. Petroff, Phys. Rev. B **41**, 12 307 (1990).

[3] C. G. Smith, M. Pepper, R. Newbury, H. Ahmed, D. G. Hasko, D. C. Peacock, J. E. F. Frost, D. A. Ritchie, G. A. C. Jones, and G. Hill, J. Phys. Condens. Matter **2**, 3405

(1990).
[4] H. Fang and P. J. Stiles, Phys. Rev. B **41**, 10 171 (1990).
[5] R. R. Gerhardts, D. Weiss, and U. Wulf, Phys. Rev. B **43**, 5192 (1991).
[6] A. Lorke, J. P. Kotthaus, and K. Plogg, Phys. Rev. B **44**, 3447 (1991).
[7] D. Weiss, P. Grambow, K. von Klitzing, A. Menschig, and G. Weimann, Appl. Phys. Lett. **58**, 2960 (1991).
[8] D. Weiss, M. L. Roukes, A. Menschig, P. Grambow, K. von Klitzing, and G. Weimann, Phys. Rev. Lett. **66**, 2790 (1991).
[9] G. M. Gusev, Z. D. Kvon, L. V. Litvin, Yu. V. Nastaushev, A. K. Kalagin, and A. I. Toropov, J. Phys. Condens. Matter **4**, L269 (1992); Superlatt. Microstruct. **13**, 383 (1993); **13**, 263 (1993).
[10] G. Berthold, J. Smoliner, V. Rosskopf, E. Gornik, G. Böhm, and G. Weimann, Phys. Rev. B **45**, 11 350 (1992); **47**, 10 383 (1993).
[11] G. M. Sundaram, N. J. Bassom, R. J. Nicholas, G. J. Ress, P. J. Heard, P. D. Prewett, J. E. F. Frost, G. A. C. Jones, D. C. Peacock, and D. A. Ritchie, Phys. Rev. B **47**, 7348 (1993).
[12] R. Schuster, K. Ensslin, J. P. Kotthaus, M. Holland, and C. Stanley, Phys. Rev. B **47**, 6843 (1993).
[13] D. Weiss, K. Richter, A. Menschig, R. Bergmann, H. Schweizer, K. von Klitzing, and G. Weimann, Phys. Rev. Lett. **70**, 4118 (1993).
[14] F. Nihey and K. Nakamyra, Physica B **184**, 398 (1993).
[15] R. Schuster, K. Ensslin, D. Wharam, S. Kühn, J. P. Kotthaus, G. Böhm, W. Klein, G. Tränkle, and G. Weimann, Phys. Rev. B **49**, 8510 (1994).
[16] T. Deruelle, B. Meurer, Y. Guldner, J. P. Vieren, M. Riek, D. Weiss, K. von Klitzing, K. Eberl, and K. Ploog, Phys. Rev. B **49**, 16 561 (1994).
[17] A. H. MacDonald, Phys. Rev. B **29**, 6563 (1984).
[18] D. Pfannkuchhe and R. R. Gerhardts, Phys. Rev. B **46**, 12 606 (1992).
[19] R. Fleischmann, T. Geisel, and R. Ketzmerick, Phys. Rev. Lett. **68**, 1367 (1992).
[20] E. M. Baskin, G. M. Gusev, Z. D. Kvon, A. G. Pogosov, and M. V. Entin, JETP Lett. **55**, 678 (1992).
[21] H. Silberbauer, J. Phys. Condens. Matter **4**, 7355 (1992).
[22] G. Kirczenow, Phys. Rev. B **46**, 1439 (1992); B. L. Johnson, C. Barnes, and G. Kirczenow, *ibid.* **46**, 15 302 (1992).
[23] S. Ishizaka, K. Nakatura, and T. Ando, Phys. Rev. B **48**, 12 053 (1993).
[24] R. B. S. Oakeshott and A. MacKinnon, J. Phys. Condens. Matter **5**, 6991 (1993); **5**, 6983 (1993); **5**, 6971 (1993).
[25] R. W. Tank and R. B. Stinchcombe, J. Phys. Condens. Matter **5**, 5623 (1993).
[26] Y. Tan, Phys. Rev. B **49**, 1827 (1994).
[27] R. B. S. Oakeshott and A. MacKinnon, J. Phys. Condens. Matter **6**, 1519 (1994).
[28] D. Hofstadter, Phys. Rev. B **14**, 2239 (1976).
[29] C. W. J. Beenakker and H. van Houten, in *Solid State Physics, Advances in Research and Applications*, edited by H. Ehrenreich and D. Turnbull (Academic, San Diego, 1991), Vol. 44.
[30] R. Landauer, Phys. Lett. **85A**, 91 (1981); M. Büttiker, Phys. Rev. Lett. **57**, 1761 (1986); R. Landauer, J. Phys. Condens. Matter **1**, 8099 (1989); A. D. Stone and A. Szafer, IBM J. Res. Dev. **32**, 384 (1988).
[31] D. S. Fisher and P. A. Lee, Phys. Rev. B **23**, 6851 (1981).
[32] J. Skjånes, G. Schön, and E. H. Hauge, Phys. Rev. B **50**, 8636 (1994).
[33] F. Sols, M. Macucci, U. Ravaioli, and K. Hess, Appl. Phys. Lett. **54**, 350 (1989); J. Appl. Phys. **66**, 3892 (1989).
[34] T. Ando, Phys. Rev. B **44**, 8017 (1991).
[35] E. Brown, Phys. Rev. **133**, A1038 (1964); J. Zak, *ibid.* **134**, A1607 (1964).
[36] L. D. Landau and E. M. Lifshitz, *Quantum Mechanics* (Pergamon Press, Oxford, 1965).
[37] P. F. Bagwell and T. P. Orlando, Phys. Rev. B **40**, 1456 (1989).
[38] A. Kumar, S. E. Laux, and F. Stern, Phys. Rev. B **42**, 5166 (1990).